



LAWRENCE
LIVERMORE
NATIONAL
LABORATORY

The NIF X-ray Spectrometer (NXS) calibration campaign at Omega

F. Perez, G. Kemp, S. Regan, M. Barrios, J. Pino, H. Scott, S. Ayers, H. Chen, J. Emig, M. Bedzyk, M. Shoup, A. Agliata, N. Izumi, K. B. Fournier

May 19, 2014

High-Temperature Plasma Diagnostics (HTPD 2014)
Atlanta, GA, United States
June 1, 2014 through June 5, 2014

Disclaimer

This document was prepared as an account of work sponsored by an agency of the United States government. Neither the United States government nor Lawrence Livermore National Security, LLC, nor any of their employees makes any warranty, expressed or implied, or assumes any legal liability or responsibility for the accuracy, completeness, or usefulness of any information, apparatus, product, or process disclosed, or represents that its use would not infringe privately owned rights. Reference herein to any specific commercial product, process, or service by trade name, trademark, manufacturer, or otherwise does not necessarily constitute or imply its endorsement, recommendation, or favoring by the United States government or Lawrence Livermore National Security, LLC. The views and opinions of authors expressed herein do not necessarily state or reflect those of the United States government or Lawrence Livermore National Security, LLC, and shall not be used for advertising or product endorsement purposes.

The NIF X-ray Spectrometer (NXS) calibration campaign at Omega

F. Pérez,^{1, a)} G. E. Kemp,^{1, b)} S. P. Regan,² M. A. Barrios,¹ J. Pino,¹ H. Scott,¹ S. Ayers,¹ H. Chen,¹ J. Emig,¹ M. Bedzyk,² M. Shoup,² A. Agliata,² N. Izumi,¹ and K. B. Fournier¹

¹⁾ Lawrence Livermore National Laboratory, P. O. Box 808, Livermore, CA 94551, USA

²⁾ University of Rochester, Laboratory for Laser Energetics, Rochester, NY 14623, USA

(Dated: 19 May 2014)

The calibration campaign of the NIF X-ray Spectrometer (NXS) was carried out at the OMEGA laser facility. X-ray line-emission spectra from various high-Z emitters, between 2 and 18 keV, were recorded by both NXS and two other spectrometers for cross-calibration. We report on the design and performance of this campaign with comparisons to radiation hydrodynamics simulations.

The National Ignition Facility (NIF) X-ray Spectrometer ‘NXS’ will record calibrated, time-resolved x-ray spectra in the 2 to 18 keV photon energy range. It consists of elliptically-bent Bragg-reflection crystals. The energy range is divided in ten partially overlapping windows, each corresponding to one given crystal configuration. For each spectral window, three identical NXS assemblies are built, thus a total of thirty assemblies. On NIF, a streak camera¹ will provide temporal resolution between 8 and 160 ps for a time window from 1 to 20 ns.

The absolute calibration of the NXS instrument was carried out at the OMEGA laser facility, replacing NIF’s streak camera with an image plate (time-integrated measurement). Within two shot days, 27 shots were taken, fielding three NXS assemblies on each shot: all thirty assemblies of NXS have acquired spectra at least twice. Simultaneously, two absolutely-calibrated x-ray spectrometers ‘XRS’ were fielded in order to cross-calibrate each NXS crystal, as shown in Fig. 1.

To generate the x-ray spectra in this calibration campaign, a target design has been carefully developed. As the instruments are fielded around the target in different directions, uniform x-ray emission was required. This implies spherical targets, uniformly irradiated by the OMEGA lasers. The calculated irradiation is 10^{15} W/cm² and its uniformity is shown in Fig. 1 (right panel). It corresponds to the sixty laser beams (1-ns, 0.5-TW square

pulses), with phase plates adapted to the 1-mm-diameter spheres. To ensure a steady target size (not imploding), full glass beads were selected instead of shells.

The x-ray spectra required line emission instead of continuum in order to provide contrast that can be discriminated against potential background. To this goal, various metals were coated on the surface of the beads. As these metals must all be ablated during the laser irradiation to emit x rays, they were coated as a mixture instead of layers. The 1.5 μ m thickness of this metallic mixture was determined using the simulations described below, to make sure that maximum emission was produced.

The ten NXS configurations span ten different x-ray-energy ranges from 2 to 18 keV. A number of metal coatings were selected (Si, Ti, Cr, Ni, Zn, Zr, Mo and Ag) to produce line emission in this whole range using their K-shell or the L-shell lines. To facilitate the target fabrication, only two or three metals could be coated on a single bead, and only a few different types of targets could be built. According to these constraints, we designed four different mixtures, denoted by A, B, C, and D, summarized in Table I. Each mixture is adapted to the x-ray range of two or three different NXS configurations, so that all ten configurations can detect line-emission from

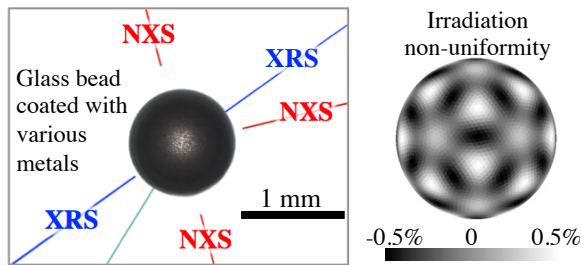


FIG. 1. (Color online) Calibration campaign setup.

TABLE I. Target composition, thicknesses (δr) and corresponding NXS crystal configurations

Target	Coating %	δr [μ m]	NXS configurations
A	Si/Mo/Ag 41/28/31	1.4	#1 from 1.9 to 2.4 keV #2 from 2.2 to 2.9 keV #3 from 2.6 to 3.7 keV
B	Ti/Cr/Ag 30/35/35	1.7	#4 from 3.0 to 4.6 keV #5 from 3.6 to 6.1 keV
C	Cr/Ni/Zn 33/33/34	1.3	#6 from 5.9 to 7.4 keV #7 from 6.7 to 8.9 keV #8 from 7.9 to 11.1 keV
D	Zn/Zr 48/52	1.6	#9 from 8.9 to 13.7 keV #10 from 10.8 to 18.2 keV

^{a)}perez75@llnl.gov

^{b)}kemp10@llnl.gov

one of these mixtures. In order to have similar magnitudes of these various x-ray lines, similar concentrations of all metals were requested, as simulations confirmed.

These targets were fabricated by General Atomics (La Jolla, CA, USA). The bead radius was measured to 0.6% precision with a microscope. The thickness of the coating and its composition were determined with 7% and 1.5% respective uncertainties using Raman backscatter analysis. All spectra were recorded on FUJI SR-type image plates.

Two sets of simulations, with two different codes, were performed to design and address the performance of each target configuration. Simulations were performed in 1D with spherical geometry using HYDRA², a multiphysics arbitrary Lagrangian-Eulerian (ALE) multi-dimensional radiation-hydrodynamics code. In an earlier stage of the design process, simulations using the ARES code had also been performed in the same geometry.

Targets A–D were modeled after the experiment with a 0.1 cm diameter solid SiO₂ bead ($\rho = 2.65 \text{ g/cm}^3$) with 1.5 μm of the previously discussed mid-Z coating. In HYDRA, the glass and coatings were treated using the Livermore equation of state (LEOS) tables and the Thomas-Fermi based quotidian equation of state (QEOS³) model, respectively. We used atomic-fraction-weighted atomic numbers $\bar{Z} = \sum_i f_i Z_i$ and atomic weights $\bar{A} = \sum_i f_i A_i$ with pressure equilibrated⁴ (harmonically averaged) mass densities $1/\bar{\rho} = \sum_i f_i/\rho_i$ and sound speeds $1/\bar{c}_s = \sum_i f_i/c_{s,i}$; a summary the QEOS input parameters for each target configuration is shown in Table II. In ARES, LEOS were used for all elements, averaging by atomic fraction.

TABLE II. QEOS input parameters in the HYDRA simulations for the various target compositions.

Target	\bar{Z}	\bar{A}	$\bar{\rho}$ [g/cm ³]	\bar{c}_s [cm/ μs]
A	32.17	72.05	4.32	0.46
B	31.45	70.32	6.73	0.40
C	27.36	50.76	7.66	0.39
D	35.20	78.82	6.80	0.34

The simulations were performed in the purely Lagrangian formulation and strict mass-matching was observed across the glass/high-Z interface (*i.e.* $\rho_1 \delta r_1 = \rho_2 \delta r_2$). The 3ω laser was treated using the 1D version of the 3D ray-tracing algorithm⁵ in HYDRA, and with a similar approach in ARES.

Guided by the model developed by Colvin *et al*⁶, HYDRA employs the Lee-More electron thermal conductivity formulation⁷ with a large flux limiter ($f = 0.2$) to account for non-local electron transport, non-LTE rates with detailed super-configuration atomic models (DCA) from CRETIN⁸, and implicit Monte Carlo (IMC) photonics for radiation transport⁹ with $\sim 10^6$ photons and

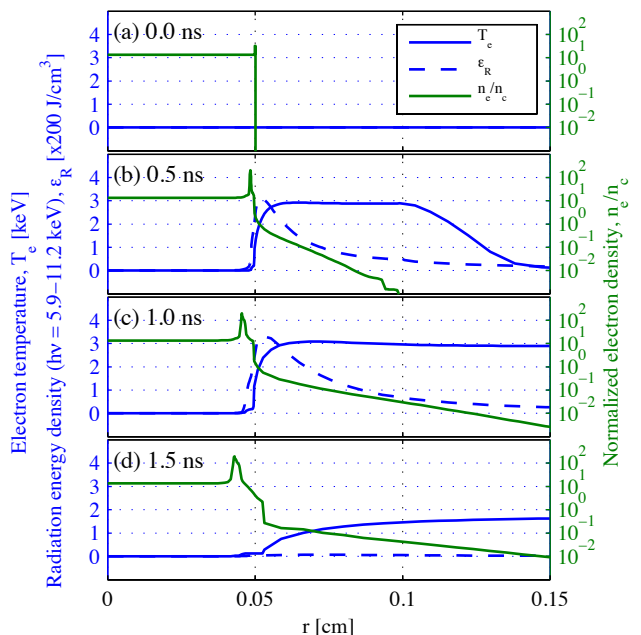


FIG. 2. (Color online) HYDRA-simulated profiles of electron temperature T_e , radiation energy density ε_R in the 5.9–11.2 keV band and electron density n_e (normalized to the critical density n_c), for target type C.

~ 480 radiation bins. ARES simply uses the Lee-More model without flux limiter, radiation diffusion with 60 bins, LTE rates, and a multi-group opacity model. It uses CRETIN only to post-process the x-ray spectra.

Overall, the HYDRA results proved to match the data better than the early ARES simulations; for this reason, we will mostly discuss the former. Shown in Fig. 2 is the spatially resolved evolution of the electron temperature T_e , radiation energy density ε_R in the 5.9–11.2 keV band (approximately NXS configurations #6 to #8) and the electron density n_e (green), normalized to the critical density $n_c \approx 9.9 \times 10^{21} \text{ cm}^{-3}$, for the target type C simulation. Throughout the simulation, we observe peak electron temperatures in the under-dense blowoff plasma ($\lesssim 0.2n_c$, $\sim 150 \mu\text{m}$ from the initial solid density interface) of approximately 3 keV and the radiation energy density is peaked at $\sim 0.5n_c$ and $\sim 2.5 \text{ keV}$ ($\sim 25 \mu\text{m}$ from the initial solid density interface). Additionally, power emitted into this band dies rapidly after the laser turns off at $\sim 1.5 \text{ ns}$. At this time, nearly 90% (by mass) of the coating for this target has become sub-critical indicating that the laser didn't completely ablate away the layer. Target types B and D performed similarly with $\sim 70\%$ ablated away by the end of the pulse whereas the coating of target type A had completely been burnt through $\sim 0.25 \text{ ns}$ before the pulse turned off.

The HYDRA x-ray spectra are reconstructed from a spherical harmonic decomposition of the IMC photons, recorded as they pass through a diagnostic sphere lo-

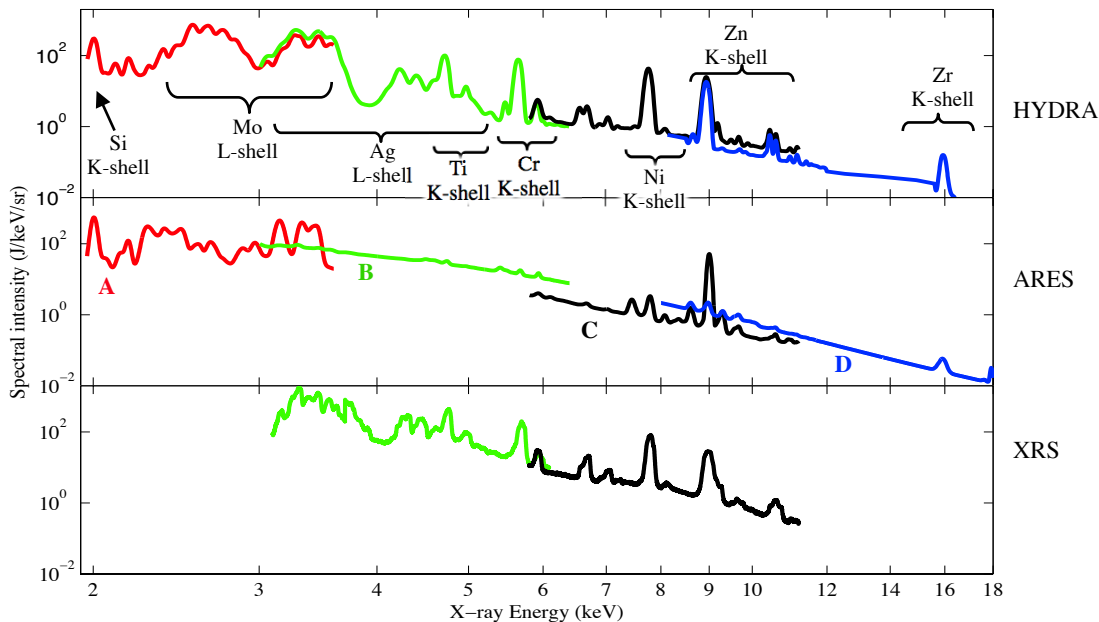


FIG. 3. (Color online) Simulated spectra for targets A to D in J/keV/sr are given for both codes, as well as experimental spectra from the XRS spectrometer.

cated at the boundary of the simulation ($r \approx 0.5$ cm). The simulated laser-to-x-ray conversion efficiency in each x-ray range of interest (see Table I) for targets A to D amounts to 19%, 14%, 1.2% and 0.3%, respectively. Integrated from 0 to 20 keV, the efficiency varies between 45 and 60%.

Figure 3 provides the four simulated spectra in absolute units corresponding to the four target types, together with a few experimental spectra from the calibrated XRS spectrometer. Line locations and ratios are overall in good agreement with the HYDRA simulations. Note that this comparison is preliminary, as the image plate response for the XRS spectra shows significant uncertainty in the range of interest. Results from the ARES code show poorer agreement, due to the reduced hydrodynamics and atomic physics models employed.

Future publications will report the NXS spectra that have been acquired during this campaign, and the corresponding calibration analysis. To this goal, the XRS spectra will be analyzed thoroughly, especially concerning the response of the image-plate detectors, which will be precisely characterized in the x-ray range of interest with gamma sources.

Overall, we described the target design that lead to a successful calibration campaign of the NXS instrument. All crystals have acquired spectra and will be cross-calibrated to the absolutely-calibrated XRS instru-

ment. The reflectivity and surface quality of each crystal will then be reported for use on NIF experiments.

This work was performed under the auspices of the U.S. Department of Energy by Lawrence Livermore National Laboratory under Contract DE-AC52-07NA27344 and supported by the Defense Threat Reduction Agency under IAA 10027-5009 BASIC, “DTRA time-resolved x-ray spectrometer for the National Ignition Facility”.

- ¹Y. P. Opachich, D. H. Kalantar, A. G. MacPhee, J. P. Holder, J. R. Kimbrough, P. M. Bell, D. K. Bradley, B. Hatch, G. Brienza-Larsen, C. Brown, C. G. Brown, D. Browning, M. Charest, E. L. Dewald, M. Griffin, B. Guidry, M. J. Haugh, D. G. Hicks, D. Homoele, J. J. Lee, A. J. Mackinnon, A. Mead, N. Palmer, B. H. Perfect, J. S. Ross, C. Silbernagel, and O. Landen, *Rev. Sci. Instrum.* **83**, 125105 (2012).
- ²M. M. Marinak, G. D. Kerbel, N. A. Gentile, O. Jones, D. Munro, S. Pollaine, T. R. Dittrich, and S. W. Haan, *Phys. Plasmas* **8**, 2275 (2001).
- ³R. M. More, K. H. Warren, D. A. Young, and G. B. Zimmerman, *Phys. Fluids* **31**, 3059 (1988).
- ⁴P. Sterne, private communication (2013).
- ⁵T. B. Kaiser, *Phys. Rev. E* **61**, 895 (2000).
- ⁶J. D. Colvin, K. B. Fournier, J. Kane, S. Langer, M. J. May, and H. A. Scott, *High Energy Density Phys.* **7**, 263 (2011).
- ⁷Y. T. Lee and R. M. More, *Phys. Fluids* **27**, 1273 (1984).
- ⁸H. Scott and S. Hansen, *High Energy Density Phys.* **6**, 39 (2010).
- ⁹J. A. Fleck, Jr. and J. D. Cummings, Jr., *J. Comput. Phys.* **8**, 313 (1971).